ISSN: 1698-6180
www.ucm.es/info/estratig/journal.htm

Journal of Iberian Geology 32 (2) 2006: 175-196

Journal of Iberian Geology
AN INTERNATIONAL PUBLICATION OF EARTH SCIENCES

Mechanisms of gas transport in clay barriers

Mecanismos de transporte de gas en barreras de arcilla

E.E. Alonso, S. Olivella, D. Arnedo

Departamento de Ingeniería del Terreno, Cartográfica y Geofísica, Universidad Politécnica de Cataluña, Barcelona, Spain

Corresponding author: eduardo.alonso@upc.edu

Received: 07/03/06 / Accepted: 13/06/06

Abstract

Laboratory experiments show that preferential paths develop through saturated impervious clay bodies. A procedure to integrate gas transmission discontinuities into a general THM formulation is described. The technique has been incorporated into a general purpose FE THM code (CODE_BRIGHT) and it has been used to reproduce gas transmission experiments in specimens. The experimentally observed peaks in gas pressure and flow rates, when breakthrough conditions are reached, are reproduced. The paper discusses also the role of local heterogeneity in gas migration. A computational experiment, inspired in the conditions prevailing on the "in situ" large scale GMT test, has been preformed. All the elements of the discretization include an embedded discontinuity. The analysis shows that small variability in buffer properties enhances the development of preferential paths.

Keywords: gas migration, clay buffers, model, discontinuity, finite element, intrinsic permeability, fracture.

Resumen

Los ensayos de flujo de gas sobre muestras saturadas e impermeables indican la formación de sendas preferenciales de circulación del gas. El artículo describe un procedimiento para integrar esas discontinuidades en una formulación general THM tal y como se desarrolla en el Programa de elementos finitos CODE_BRIGHT. Con esta técnica se ha reproducido el comportamiento observado en muestras ensayadas. Se consigue reproducir los máximos observados en la presión de inyección y en el flujo de descarga cuando se abre por primera vez un camino preferencial. El artículo discute también el papel de la heterogeneidad a pequeña escala en el flujo de gas. Se ha desarrollado un experimento computacional inspirado en la geometría, materiales de barrera y condiciones de contorno del ensayo a gran escala GMT, desarrollado en el Laboratorio de Grimsel. Todos los elementos de la discretización incluyen discontinuidades embebidas. El análisis muestra que la pequeña variabilidad de propiedades de la barrera facilita el desarrollo de caminos preferenciales al flujo de gas.

Palabras clave: migración de gas, barrera de arcilla, modelo, discontinuidad, elemento finito, permeabilidad intrínseca, fractura.

1. Introduction

Current understanding of physical phenomena taking place in an engineered clay barrier seems to provide a satisfactory answer to most of the questions which may be raised in design and performance evaluation exercises. This positive situation is the result of decades of intense research effort. Theoretical and numerical developments, laboratory experimental research and large scale demonstration experiments have contributed to establishing a solid knowledge of the thermo-hydro-mechanical behaviour of compacted clay buffers, and, more specifically, those integrated by compacted bentonite blocks. A recent account of the large scale and demonstration experiments involving bentonite barriers in granitic host rock is given in Alonso and Ledesma (2004).

Most of the research work performed in the THM behaviour of barriers concerns the initial transient processes of hydration under the combined action of the infiltrating water from the host rock and the heat generated by the canister. For obvious reasons, the experimental information concerning this transient process only covers a minimum time period of the expected lifetime of an engineered barrier. In the demonstration project FEBEX, probably the most complete large scale experiment conducted so far, "only" seven years of field data are available.

The long term behaviour of clay barriers has received comparatively less attention. Processes or phenomena taking place have to be extrapolated from the known behaviour during the transient phase, on the basis of the basic understanding of material behaviour, including here the bentonite but also the canister and host media.

A significant issue in long term behaviour of clay buffers is its capability to maintain tightness under the expected generation of gases due to canister corrosion and other phenomena. Current research in this important topic, directly related to the long term safety evaluation of a repository, concentrates in understanding the mechanisms of gas transport through a mass of saturated, compacted bentonite, under the confinement stress provided by the host rock.

A large proportion of the experimental research performed concerns laboratory tests of gas flow through compacted specimens, fully hydrated. They play the role of "point" tests, although, as explained later, they can be hardly interpreted if they are considered in the Cauchy sense of a homogeneous, small specimen able to provide fundamental constitutive behaviour. Large scale tests have rarely been conducted. The experience gained during the analysis of the large Gas Migration Test (GMT) performed in Grimsel has shown that there are no reliable procedures to track the path of gas through a saturated impervious buffer. It turns out that the performance of a large experiment is very sensitive to "minor" details, such as the presence of joints, interfaces or buffer layers. From a theoretical standpoint difficulties also arise because the classical framework for THM analysis, which solves the equations of mass, heat and momentum balance in a porous medium, are insufficient to take into account the development of preferential gas paths through the barrier. In fact, preferential paths take place, under some circumstances of imposed flow rate or gas pressure and stress state, in laboratory specimens, i.e. at a very small scale. The problem of path opening is part of the solution sought and this situation poses a major difficulty to modelling work.

This paper reviews some aspects of the mechanisms of gas transport in saturated compacted bentonite. A review of some relevant laboratory experiments is first made. They provide a convenient background for the remaining of the paper and emphasize the role played by preferential paths in gas migration. A model put forward by the authors, to simulate the concentrated flow of gas, is then outlined. One advantage of the model is that it can be implemented, at a limited effort, in general purpose THM finite element codes such as CODE_BRIGHT (DIT-UPC, 2000). The performance of the model (described as a "cracking continua") to simulate tests on specimens is then illustrated.

The large scale GMT test is then presented. Its purpose was the analysis of gas migration through a compacted barrier of sand/bentonite (80/20). The test results and the modelling performed will not be described in detail here (see however, Olivella and Alonso, 2005). A particular aspect will be highlighted here: the relevance of heterogeneity to explain the formation of singular gas paths. To do so, the main transmission zone in GMT has been represented by means of a randomly heterogeneous field of "cracking" elements. In this way the two phenomena which are believed to play a fundamental role in gas migration: the local heterogeneity and the possibility of generating paths of high transmissivity are combined into a single formulation. Some computational results are discussed on the light of the data recorded in the real scale experiment.

2. Some experimental observations

The main characteristics of a few recent laboratory tests performed on compacted specimens of bentonite have been summarized in Table 1. Some relevant results will be presented here.

Authors	Bentonite	Dry Density (Mg m^{-3})	Flow geometry	Gas Flow Controls	Confining Conditions
Pusch and Forsberg (1983) ‡	MX80	~1.35-1.65*	Linear	Constant pressure / pressure increments	Constant volume oedometer
Pusch *et al*. (1985)	MX80	~1.1-1.78*	Linear	Pressure increments	Constant volume oedometer
Horseman and Harrington (1997)	MX80	1.5-1.7	Linear (axial) flow	Displacement of gas by water from an upstream reservoir.	Constant isotropic stress in flexible sleeve subject to external fluid pressure (8-22 MPa)
Horseman and Harrington (1997)	MX80 paste	1.3-1.4	Point source and sink	Displacement of gas by water from reservoir.	Cylindrical pressure vessel with confining pressure (0.8-2.7 MPa) imposed on floating end cap
Tanai *et al.* (1997)	Kunigel VI, Fo-Ca Clay	1.4-1.8	Linear	Pressure increments	Constant volume cylinder
Gallé (1998; 2000)	Fo-Ca Clay	1.6-1.9	Linear	Pressure increments	Constant volume oedometer cell
Graham *et al.* (2002) Hume (1999)	Avonlea	0.6-1.4	Linear	Pressure increments	Constant volume oedometer cell
Harrington and Horseman (2003)	MX80	1.577-1.582	Approximately radial from central source	Displacement of gas by water from an upstream reservoir.	Constant volume cylindrical vessel.
Harrington and Horseman (2003)	MX80	1.596	Linear	Displacement of gas by water from an upstream reservoir.	Cylindrical pressure vessel with confining pressure (10 MPa) applied to floating end caps.
Tanai (unpublished 2002)	MX80	1.63	Linear	Constant gas pumping rate	Constant isotropic stress in flexible sleeve subject to external fluid pressure

Table 1.- Summary of experiments on gas migration in compacted Bentonite. GAMBIT Workshop, Madrid, 2003.
Tabla 1.- Resumen de los ensayos sobre la migración de gas en bentonita compactada. GAMBIT Workshop, Madrid, 2003.

2.1. Horseman and Harrington (1997; 1999) tests

Seven gas migration tests were performed on cylindrical samples of compacted MX-80 bentonite. Samples were divided in two groups, HS (high swelling, 4 samples) and MS (medium swelling, 3 samples). Samples were first saturated and consolidated under different values of isotropic confining stress and a water backpressure of 1MPa. Afterwards, gas injection started at different values of (constant) flow rate. Injection pressure and flow rate out of the specimen were monitored during the tests.

The high swelling specimens had void ratios in the range 0.64-0.66 (γ_d = 1.67-1.69 Mg/m^3), swelling pressures in the range 14.8-17.1 MPa and intrinsic permeability around 0.5-0.6 10^{-20} m^2. The medium swelling specimens had void ratios in the range 0.72-0.78 (γ_d = 1.55-1.60 Mg/m^3), swelling pressures in the range 6.4-9.3 MPa and intrinsic permeability around 10^{-20} m^2. Swelling pressures and intrinsic permeabilities were estimated from published trends (Börgesson *et al*., 1996).

Samples had a diameter and heights of 49mm. Specimens were tested in a cell under isotropic stress conditions. The apparatus is described in detail in Horseman and Harrington (1997), Horseman *et al*. (1999).

Specimens were fully saturated (S_r>99%) and equilibrated under confining stress with a backpressure of 1.0 MPa applied at both ends. Net flows were monitored to establish the point of equilibration. Helium gas was injected at constant flow rate.

The volumetric flow rate of the injected fluid and the pressure of the downstream fluid were controlled using two syringe pumps. A pressure transducer monitored the outgoing pressure.

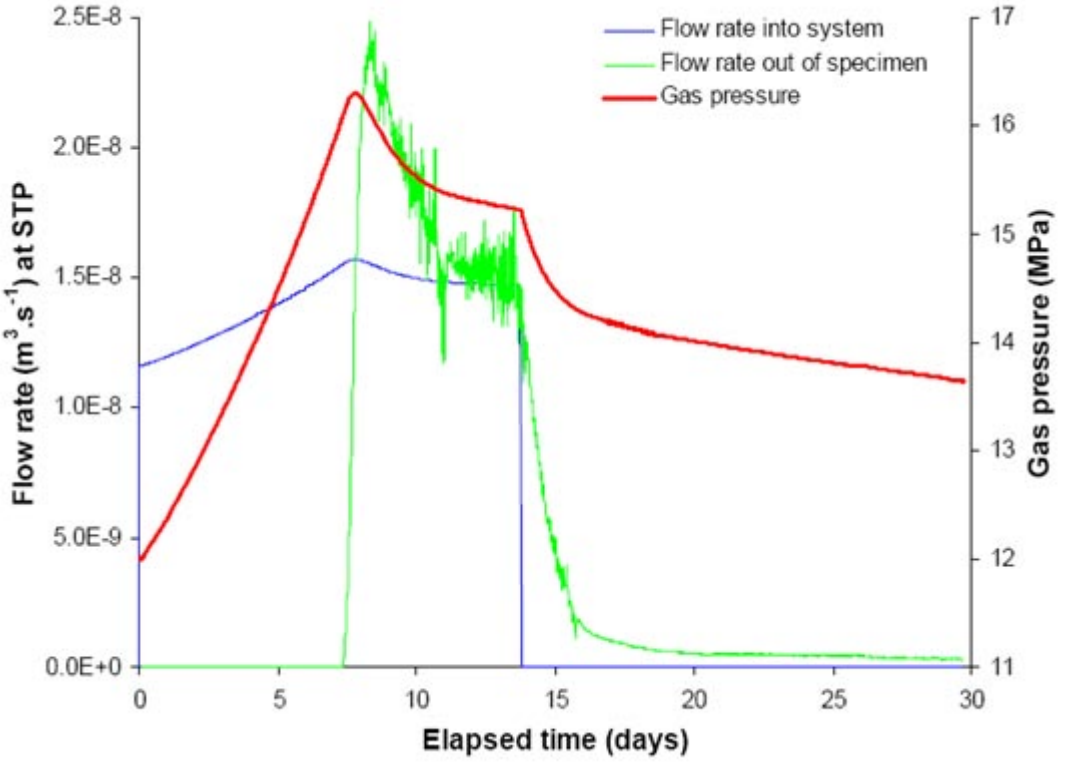

Fig. 1.- Evolution of flow rate into system, injection pressure and outgoing flux during the first injection and shut-in stage. Test MX80-4A. Horseman and Harrington (1999).

Fig. 1.- Evolución del caudal entrante, presión de inyección y flujo de salida durante la primera inyección y la fase de cierre. Ensayo MX80-4A. Horseman and Harrington (1999).

The test on specimen MX80-4A (high swelling) is representative of the experimental findings. The applied confining stress was 16.0 MPa. A gas breakthrough event was detected approximately at day 7 after the beginning of the injection. Gas injection was stopped at day 14 and the shut-in transient was monitored. Gas injection was re-started at day 30 at the same value of flow rate. After the second gas injection stage the specimen was subjected to a decreasing history of pumping rates: 180, 90, 45 and 0 µl/h.

Figure 1 shows the first stage of test MX80-4A. Confining stress and backpressure were 16.0 and 1.0 MPa, respectively. Initially gas was injected at a pumping rate of 375 µl/h. Gas breakthrough (a sudden and sharp increase in flow rate out of the sample) occurs at a gas injection pressure of 16.2 MPa. Peak injection pressure is slightly higher, 16.3 MPa. After the peak the gas pressure decreases to a steady state value of 15.22 MPa. Then gas injection is stopped.

Figure 2 shows the injection flow rate, injection pressure and outgoing flux during the remaining stages of the test. In the second injection stage the increase in flow rate out of the sample starts just as the injection pressure increases. No breakthrough pressure was determined now. The peak pressure (15.25 MPa) is lower than in the first stage, but it is very close to the previous steady-state pressure.

Horseman *et al.* (1999) reached several conclusions in their investigation. Perhaps the most relevant result is that no water displacement was observed to occur inside the specimen, despite the fact that the observed breakthrough pressure seems to be higher than the air entry pressure of the compacted bentonite. The peaks observed in gas pressure and measured flows into and out of the specimen are also quite characteristic. Such behaviour has been measured in other clay materials as well. The spontaneous decrease in pressure after the peak is taken as an indication of the aperture of a preferential path of high conductivity. The absence of a marked peak during the second injection phase indicates that the initial path remained partially open. This interpretation is also consistent with the lower gas pressure reached during the second injection phase. It was also checked that the gas pressure at peak is equal to the swelling pressure plus the existing pore pressure. In other words, the gas pressure has to reach the total stress in a critical plane in order to develop a preferential path.

This result is consistent with the experience available on the conditions of hydraulic fracture in clay cores of dams (Alonso, 1997)

In a series of oedometer tests performed on specimens of bentonite, Graham *et al.* (2002) found that the breakthrough pressure decreases as the degree of saturation decreases. Below a certain value (Sr < 0.93) the breakthrough pressure becomes a small constant value (Fig. 3). It is expected that for high degrees of saturation the gas migration takes place as a combination of two-phase flow and some preferential paths opened by the gas pressure, the second being dominant in low permeability clays.

It was also found that the time for breakthrough depends on factors such as the specimen density and the applied gas pressure.

3. A model for crack opening. A continuous body with embedded discontinuities

Gas generation due to corrosion of radioactive waste canisters and migration through the geological barriers is of major concern in the context of safety analysis. The generated gas may accumulate and, as the pressure increases, it will start flowing through the engineered barrier and eventually through the geological barrier (Gens *et al.*, 2001; Alonso *et al.*, 2002). The mechanisms of gas migration can be: diffusion, two phase flow and two phase flow coupled to mechanical effects which may lead to fracturing the porous media. While diffusion and two phase flow have been investigated in great detail, two phase flow coupled to deformation has received less attention.

The low permeability of the engineered and geological barriers implies that the capillary pressure to start desaturation (air entry pressure) will be high (small pore sizes). Then, gas pressure may increase reaching values that may lead to gas fracture processes or simply gas flow through existing discontinuities that may undergo changes in its aperture. Modeling gas flow under these conditions requires the introduction of mechanical formulations that allow taking into account fracture opening or fracturing formation plus subsequent opening.

This section describes a procedure to model in a unified manner two phase flow with concentrated gas flow through fractured porous rocks.

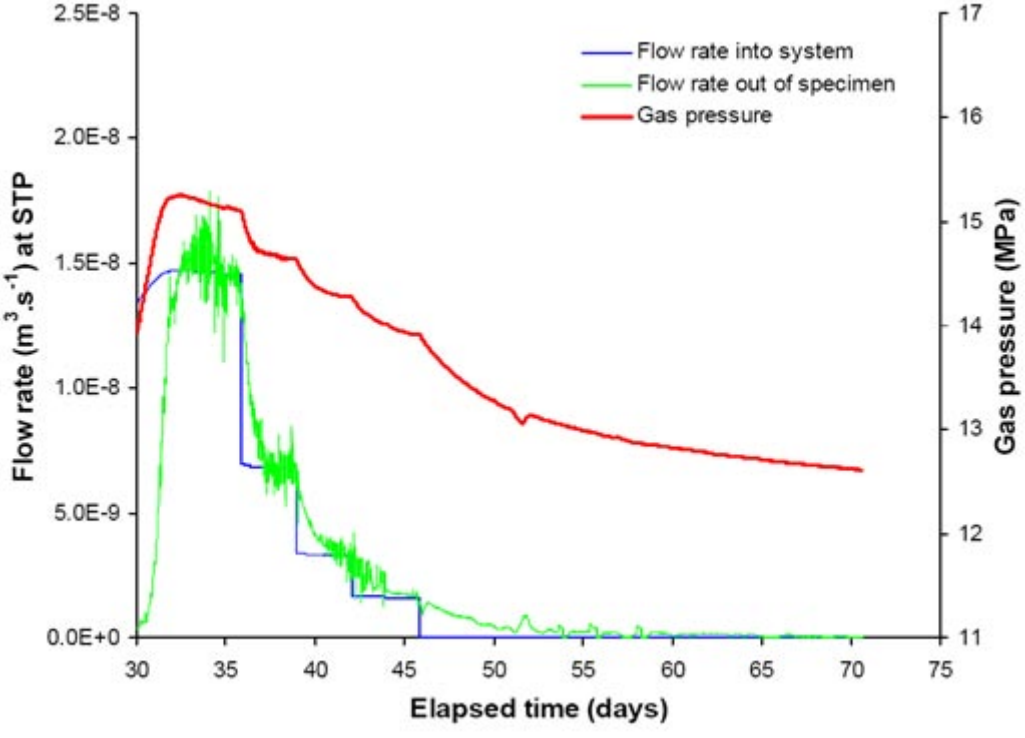

Fig. 2.- Evolution of flow rate into system, injection pressure and outgoing flux during the remaining stages. Test MX80-4A. Horseman and Harrington (1999).

Fig. 2.- Evolución del caudal entrante, presión de inyección y flujo de salida durante el resto de fases. Ensayo MX80-4A. Horseman and Harrington (1999).

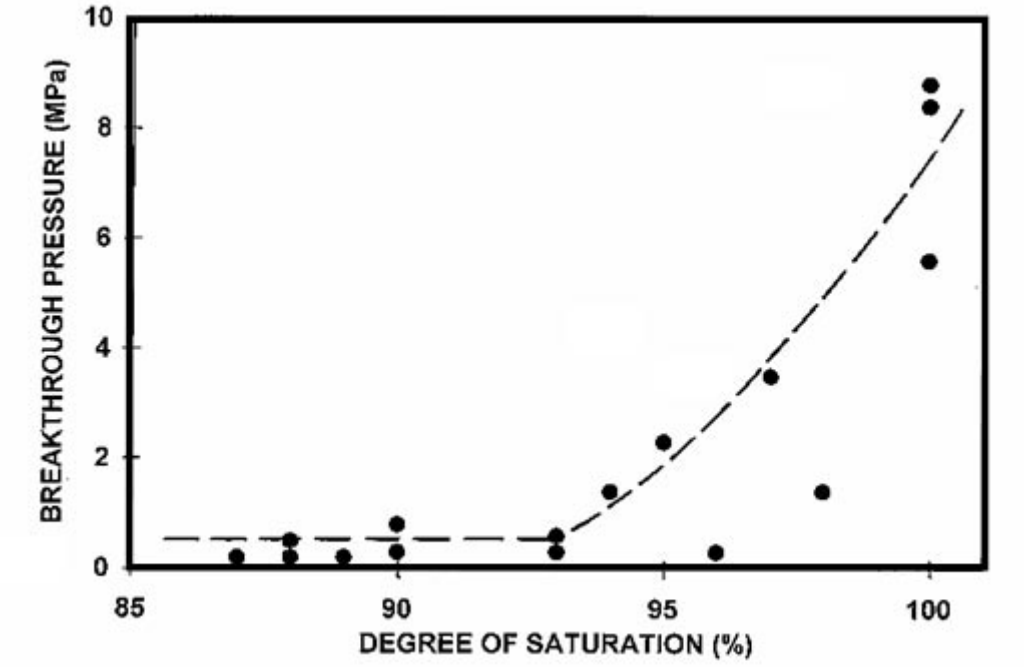

Fig. 3.- Relationship between breakthrough pressure and degree of saturation for tests on bentonite specimens reported by Graham *et al.* (2002).

Fig. 3.- Relación entre la presión de penetración y el grado de saturación de los ensayos sobre muestras de bentonita analizados por Graham *et al.* (2002).

3.1. Model description

The basic idea of the model presented here consists in the appropriate representation of single fractures embedded in a continuous finite element. Figure 4 shows a finite element composed by a rock matrix and a series of *n* fractures. The number of fractures in an element depends on the width associated with each fracture, *a*, which is a characteristic size of the material, and the element size *s*.

Hydraulic and mechanical effects have to be included because gas flow depends critically on the mechanical interactions because they control fracture aperture or porosity changes.

Consider first the flow phenomena through a single fracture. Liquid and gas flow will be calculated using Darcy's law. The most important parameter in this law is the intrinsic permeability which can be calculated, assuming laminar flow, as:

$$k_{fracture} = \frac{b^2}{12} \qquad (1)$$

where *b* is the aperture of the single fracture. In finite element applications the element size becomes a limitation for fracture modeling, because it is not convenient to use very thin elements. Alternatively, there is the possibility of considering explicit joint elements. Here it is preferred to use homogenized properties because practical applications are an objective of this work. In fact, the introduction of a set of discrete fractures tends to complicate the analysis in a significant manner.

When a set of *n* fractures is included in a finite element (Figure 4), the equivalent intrinsic permeability of the element can be calculated as:

$$k = k_{matrix}\left(\frac{s-nb}{s}\right) + \sum_{i=1}^{n}\left(k_{fracture}\frac{b}{a}\frac{a}{s}\right) =$$

$$= k_{matrix}\left(\frac{s-nb}{s}\right) + \sum_{i=1}^{n}\left(k_{fracture}\frac{b}{a}\frac{1}{n}\right) \cong k_{matrix} + \frac{b^3}{12a} \qquad (2)$$

where k_{matrix} is the reference intrinsic permeability of the matrix. In the case of gas propagation through rock the matrix refers to the rock without fractures. *s* is the element size (width normal to flow direction), *a* is the width associated with each fracture, and $n = s / a$ is the number of fractures in the element. Permeability of the matrix will be important only for very low apertures; otherwise fracture permeability will dominate the total permeability and matrix permeability will be negligible. Equation (2) shows that the element permeability does not depend on the size of the element but depends on the width associated with each fracture *a*, which can be considered a characteristic parameter for a specific medium.

The second hydraulic process that is included in the fracture is the variation of capillary pressure caused by changes in the aperture. According to Kelvin's law the

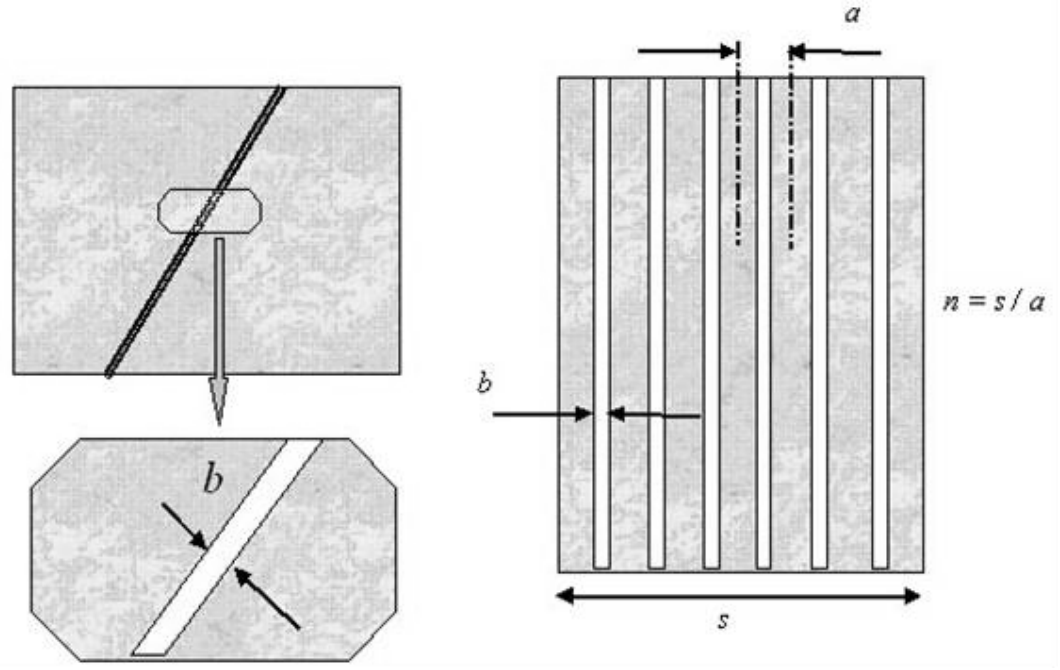

Fig. 4.- Rock with a single idealized fracture and a series of parallel fractures uniformly separated.
Fig. 4.- Roca con una única fractura idealizada y una serie de fracturas paralelas separadas de manera uniforme.

capillary pressure necessary to desaturate a fracture is given by:

$$P_o = \sigma\left(\frac{1}{r_1}+\frac{1}{r_2}\right)=\frac{2\sigma}{b} \qquad (3)$$

The second member is obtained when $(1/r_1) = 0$ and $r_2 = b/2$ (assuming that the contact angle is 0). This equation can be used directly to calculate the air entry value of the element. If Equation (3) is combined with Equation (2) the capillary pressure to start desaturation is obtained as:

$$P = P_o \frac{\sqrt[3]{k_{fracture\_o}}}{\sqrt[3]{k_{fracture}}} \qquad (4)$$

where subscript *o* refers to a reference (initial) aperture.

From the mechanical point of view, we are interested in the process of fracture formation and aperture. The aperture of the fracture can be estimated as a function of deformation in the following way:

$$b = b_o + \Delta b$$
$$\Delta b = a\Delta\boldsymbol{\varepsilon} = a(\boldsymbol{\varepsilon}-\boldsymbol{\varepsilon}_o) = (s/n)(\boldsymbol{\varepsilon}-\boldsymbol{\varepsilon}_o) \qquad (5)$$

Here, it has been assumed that deformation is localized and results in changes in aperture. A threshold value ($\boldsymbol{\varepsilon}_o$) is considered. Therefore the changes in aperture start when

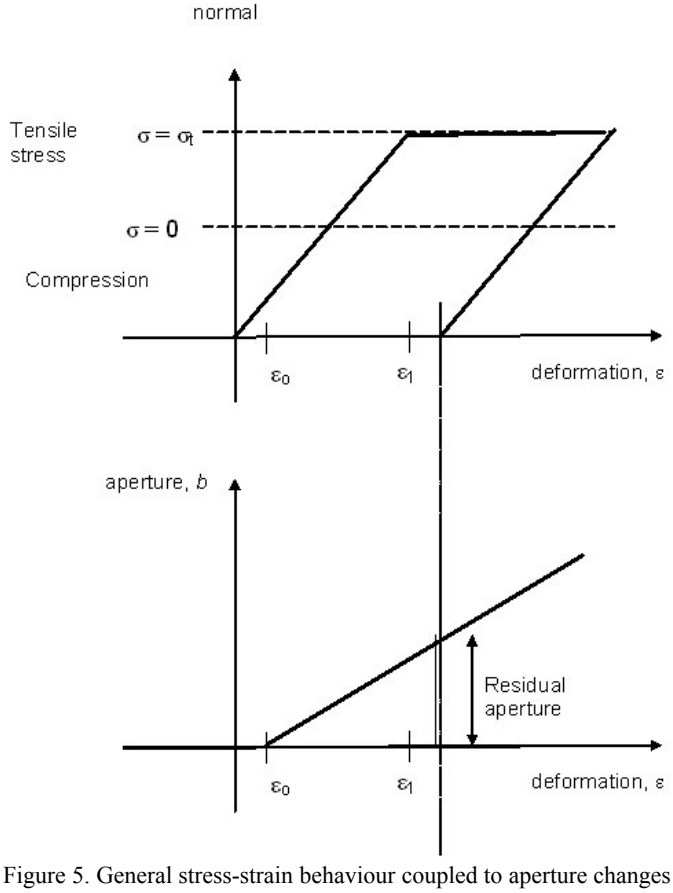

Figure 5. General stress-strain behaviour coupled to aperture changes in the case of tension opening.
Figure 5. Relación tensión-deformación general y cambios de apertura de junta en tracción.

deformation reaches this value. Deformation perpendicular to the fracture plane is used when aperture changes have to be obtained. The threshold value ($\boldsymbol{\varepsilon}_0$) is associated with fracture initiation. This parameter will be set to zero if the fractures already exist and have an initial aperture b_o. In practice, the initial aperture can be essentially zero when the fractures exist but are closed.

The stress-strain behaviour of the medium (clay barrier or rock), including fracture formation, is a crucial component of the aperture changes. As mentioned before the deformation normal to the fracture is considered in Equation (5) in order to obtain aperture changes. If an elastoplastic model is considered for the mass behaviour, fracture initiation can be associated with tension stresses or with dilatancy. On the other hand, fracture orientation is sensitive to the stress tensor orientation so the plane where the minimum principal stress (compression positive) occurs defines the plane of fracture formation. Equation (5) is introduced in Equation (2) to calculate the element permeability in the following way:

$$k = k_{matrix} + \frac{b^3}{12a} = k_{matrix} + \frac{\left(b_o + a(\boldsymbol{\varepsilon} - \boldsymbol{\varepsilon}_o)\right)^3}{12a} \qquad (6)$$

From this relationship it is clear that the element permeability depends on the fracture spacing (a), which is a characteristic parameter of the material, but is independent on the element size (s).

Normally, it will be of interest to consider $s \geq a$ (i.e. $n \geq 1$, one or more fractures in each element) because in this way, some of the elements in the finite element mesh will develop higher permeability due to opening of the fractures contained in these elements. Other elements, will maintain the properties of the intact medium. Consequently, preferential paths can be simulated. On the contrary, if $s < a$ (i.e. $n < 1$, less than one fracture in each element), a single fracture would be homogenized into various elements and a suitable smoothing of the preferential flow path would take place.

Figure 5 shows the general stress-strain behaviour coupled to aperture changes in the case of tension taking place in the medium. A threshold strain ($\boldsymbol{\varepsilon}_0$) defines the initiation of fracture aperture, as mentioned before. A strain corresponding to failure is also considered ($\boldsymbol{\varepsilon}_1$). In this case, failure is achieved when the normal stress reaches the tensile strength (σ_t). $\boldsymbol{\varepsilon}_0$, $\boldsymbol{\varepsilon}_1$ and σ_t are model parameters.

From this general model the following cases can be established:

a) Existing fracture initially closed:

$\sigma_t = 0$, $\boldsymbol{\varepsilon}_0 \approx 0$

b) Non existing fracture:

$\sigma_t \neq 0$ and $\boldsymbol{\varepsilon}_0 = \boldsymbol{\varepsilon}_1 \neq 0$

The first case (a) corresponds to a fracture, that due to compression stresses, is almost closed or has an initial aperture b_o. Normal extension will induce aperture opening right from the beginning of stressing. As the normal stress reaches a zero value, deformation will increase under constant stress (irreversible deformations). Unloading will imply fracture closure but a residual aperture is expected due to irreversible deformations. An appropriate elastic modulus could be used if complete closure had to be achieved.

The second case (b) implies that a tensile strength exists and, therefore, aperture cannot be initiated before failure by tension occurs. For this reason the threshold strain ($\boldsymbol{\varepsilon}_0$) is set equal to the strain corresponding to failure ($\boldsymbol{\varepsilon}_1$). This latter value depends on the tensile strength. Normally, failure would have to be associated with softening because the material is damaged.

Another situation takes place in case of dilatancy induced by shearing. In this case, the formation of fractures is due to extension which is a consequence of dilatancy. Again the threshold strain is convenient to define the initiation of fracture opening.

Fractures induced by tension and fractures induced by dilatancy, even though they are processes physically different are jointly considered in elastoplastic models. For instance, in critical state models extension induced by tension or extension induced by dilatancy depend essentially on the stress path followed.

This model has been implemented in CODE_BRIGHT (Olivella *et al.*, 1995) and some cases have been analysed to investigate the response of the coupled behaviour.

Further improvements of the model may incorporate different aspects such as the influence of the formation of infilling material due to shear displacements between crack interfaces. Lee and Chou (2002) have investigated the variation of intrinsic permeability when fractured rocks (granite and marble) are subjected to normal and shear deformations. This work shows that mechanical and hydraulic apertures are not always in linear trend. For instance, deviation takes place for large shear strains due to formation of infilling materials. The overall effect is that permeability was bounded by a maximum value. This effect may justify the inclusion in the model of a maximum hydraulic aperture.

The fact that this model considers elastic and inelastic fracture aperture or closure has already been discussed in the literature. For instance, Renner *et al.* (2000) investigated the behaviour of fractured argillaceous rocks

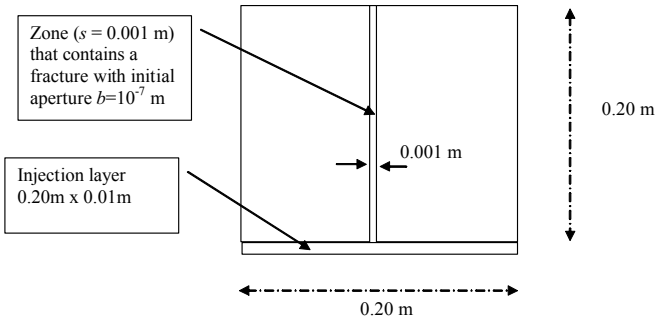

Fig. 6.- Schematic representation of the 2-D idealization of a sample containing a fracture initially closed (initial aperture 10^{-7} m).

Fig.6.- Esquema de la representación en 2-D de una muestra que contiene una fractura inicialmente cerrada (apertura inicial a 10^{-7} m).

including permeability variations induced by changes in confining pressures. In this work crack dimensions and permeability are correlated by means of a model that takes into account elastic crack closure and crack closure controlled by inelastic processes. This is explained by asperity indentation when rough crack walls contact each other.

3.2. Simulation of gas flow tests and gasfract tests

In order to study the possibilities of the model some idealized tests are presented here. The test geometry is illustrated in Figure 6.

A sample is considered with an assumed initial intrinsic permeability of 10^{-19} m^2, both in the porous medium and in the element that will contain the fracture. Capillary pressure to start desaturation (air entry value) in the porous medium is assumed to be 0.3 MPa.

Confining stress is 1 MPa (horizontal) and the initial pressure of water is 0.1 MPa (atmospheric pressure). Tensile strength in the fracture is assumed to be 0 (fracture exists before fluid injection) or 0.5 MPa (fracture does not exist before fluid injection) depending on the case. The elastic bulk modulus was assumed to be K = 1000 MPa and the elastic shear modulus was G = 1000 MPa. The initial strain to start discontinuity aperture is $\boldsymbol{\varepsilon}_o$ = 0.0. In the first case, the fracture is assumed to be present before injection of the gas starts ($\boldsymbol{\varepsilon}_1$ = 0.0 for this case because the fracture exists).

With the parameters given before, fracture opening will start immediately when the normal stress decreases. Pressures cannot exceed the confining pressure along all the fracture because in that case the fracture can freely open (tensile strength is zero). However, since there is a pressure gradient, gas pressure can be locally higher than the confining pressure. Gas flow rate at injection point is fixed at 0.0432 g/h.

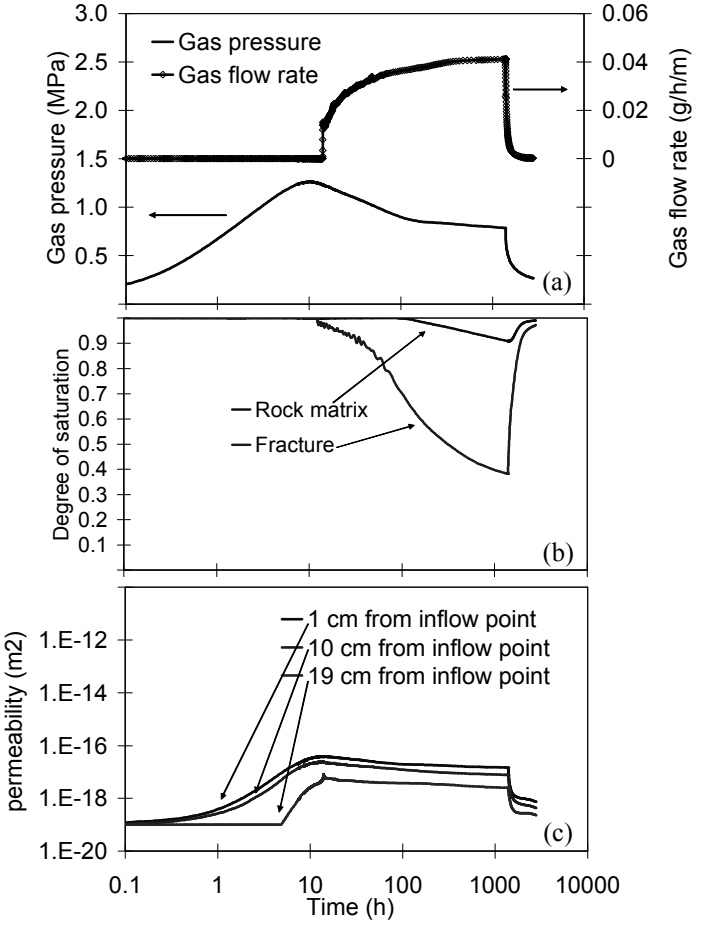

Fig. 7.- a) Gas pressure at injection point and gas flow rate at outflow point. b) Degree of saturation, c) Equivalent intrinsic permeability of the elements that contain the fracture for different distances from injection point.

Fig. 7.- a) Presión de gas en el punto de inyección y caudal de gas en el punto de evacuación. b) Grado de saturación. c) Permeabilidad intrínseca equivalente de los elementos contenidos en la fractura para diferentes distancias desde el punto de inyección.

Figure 7a shows the evolution of gas pressure at the injection point and the gas flow rate at the outflow point. It can be observed that after a period of gas pressure increase corresponding to the desaturation of the injection layer, gas starts to penetrate in the medium. Figure 7b shows degree of saturation for both the fracture and matrix. Gas flow takes place through the fracture because permeability is higher than in the matrix and because desaturation is easier than in the matrix. Due to fracture aperture, permeability increases and the air entry pressure decreases.

Finally, Figure 7c shows the evolution of intrinsic permeability as a result of fracture aperture. It can be observed that changes in permeability take place as soon as gas is injected due to the assumed existence of the fracture. For this simulated test, steady state is practically

Flow rate (g/h/m)	Maximum gas pressure (MPa)	Steady state pressure (MPa)	Comments
0.0144	0.78	0.54	Gas pressure below confining pressure
0.0288	1.14	0.67	Gas pressure below confining pressure (locally higher)
0.036	1.21	0.76	Gas pressure below confining pressure (locally higher)
0.0432	1.26	0.79	Intermediate situation
0.0576	1.36	0.1	Gas opening of the fracture along the sample due to gas pressure higher than confining pressure. Irreversible opening of the fracture
0.072	1.66	0.1	Gas opening of the fracture along the sample due to gas pressure higher than confining pressure. Irreversible opening of the fracture

Table 2.- Maximum gas pressure as a function of the injected gas flow rate.
Tabla 2.- Presión máxima de gas en función del caudal de gas inyectado.

reached after 1000 h although there is still some gas pressure dissipation.

This analysis has been performed for different values of the gas flow rate. The behaviour was similar and the maximum and steady state gas pressures achieved are included in Table 2. It can be observed that a flow rate of 0.0576 g/h produces failure, which implies large aperture of the fracture, large permeability increase, sharp drop of the gas injection pressure and, consequently, unstable numerical solution.

Figure 8 shows the peak pressure and the steady pressure (post breakthrough) as a function of gas flow rate. For low flow rates, the difference between these two pressures increases moderately. At a given point of flow rate and pressure there is a change in the behaviour because the presence of irreversible deformations in the discontinuity. In this case, the opening is large and the permeability increases substantially. Therefore, the steady state pressure is very low (practically negligible). It can be observed that the confining pressure (1

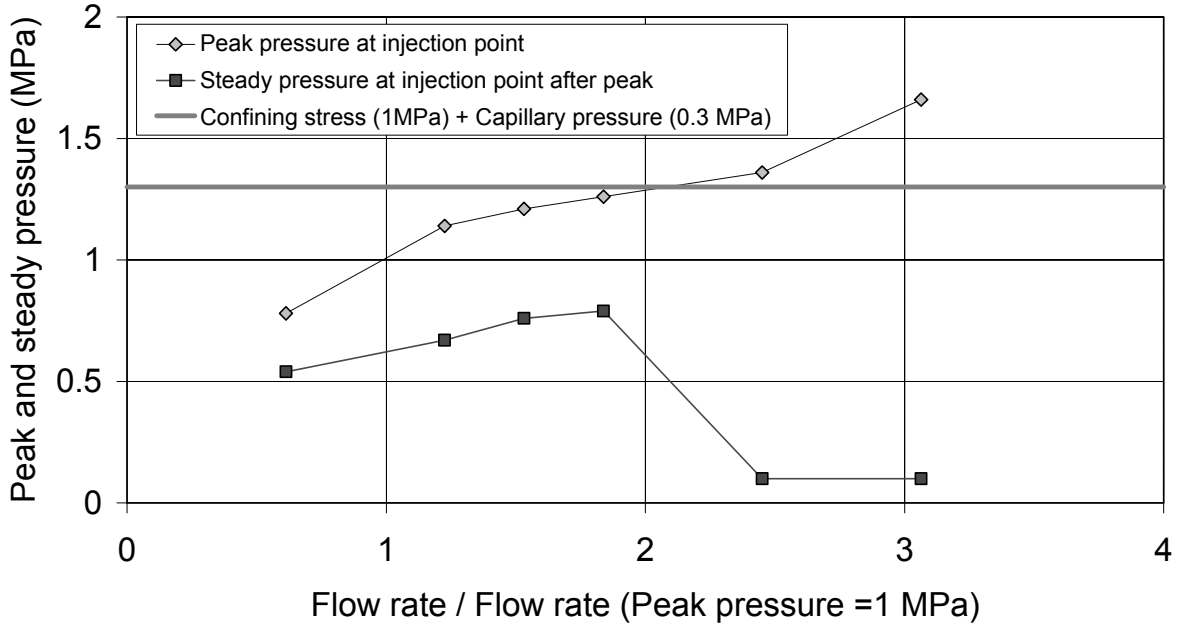

Fig. 8.- Peak and steady gas pressure at injection point for different tests at increasing injection gas flow rates. The response is reversible below 2 and irreversible above 2 because the irreversible opening of the discontinuity.
Fig. 8.- Presión de gas de pico y en condiciones estacionarias en el punto de inyección para diferentes ensayos a caudales de inyección de gas crecientes. La respuesta es reversible por debajo de 2 e irreversible por encima de 2, debido a la apertura irreversible de la discontinuidad..

MPa) and the air entry pressure (0.3 MPa) have to be overcome by the peak pressure in order to obtain irreversible opening of the fracture. Otherwise the opening is only caused by elastic changes which are induced by effective stress reduction.

The same sample is considered now in order to study the behavior of gas flow in a non-damaged material. In this second case, the fracture does not exist at the initiation of the test. Confining stress is again 1 MPa (horizontal) and the initial pressure of water and gas is 0.1 MPa (atmospheric pressure). Tensile strength in the fracture is assumed to be 0.5 MPa in this second series. The initial strain to start fracture aperture is set to 0.0001 (i.e ε_o = 0.0001 while ε_l = 0.001 for this case). This value permits a certain gas flow before fracture failure. Gas was injected in this case at 0.216 g/h, i.e. a higher flow rate than in the case of previous existing fracture.

Figure 9a shows the pressure at injection point and the gas flow rate at the extraction point. It can be observed that a sharp increase of flow rate develops which can be associated with the gas accumulation at the injection layer before the breakthrough takes place (3.7 h). This breakthrough is related to two phase flow and to fracture formation. While Figure 9b shows desaturation Figure 9c shows permeability changes due to fracture aperture. A preferential path has developed due to the increase of gas permeability caused by desaturation and deformation.

The flow rate considered for this simulation is not sufficiently high to develop a fracture failure because pressure does not reach the confining pressure plus the tensile strength along the fracture (except near the injection point). Increasing the flow rate will imply failure. The simulation has been performed for different flow rates and the maximum pressures obtained are summarized in Table 3.

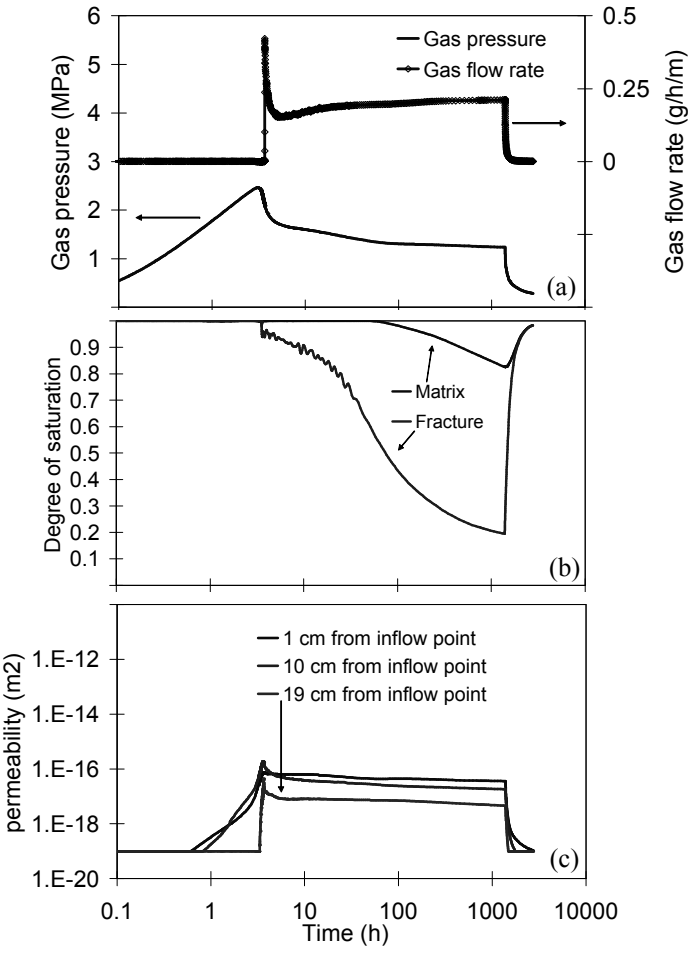

Fig. 9.- a) Gas pressure at injection point and gas flow rate at outflow point. b) Degree of saturation at the centre of the sample. c) Equivalent intrinsic permeability of the elements that contain the fracture for different distances from injection point.

Fig. 9.- a) Presión de gas en el punto de inyección y caudal de gas en el punto de evacuación. b) Grado de saturación en el centro de la muestra. c) Permeabilidad intrínseca equivalente de los elementos contenidos en la fractura para diferentes distancias desde el punto de inyección.

Flow rate (g/h/m)	Maximum gas pressure (MPa)	Steady state pressure (MPa)	Comments
0.036	1.34	0.87	No gas fracture
0.072	1.57	0.98	No gas fracture
0.144	2.02	1.14	No gas fracture
0.216	2.50	1.13	Gas fracture initiation near injection point
0.288	2.84	0.1	Gas fracture along the sample

Table 3.- Maximum gas pressure as a function of the injected gas flow rate.
Tabla 3.- Presión máxima de gas en función del caudal de gas inyectado.

Figure 10 shows the peak and steady gas pressure at the injection point for different tests at increasing injection gas flow rates. Flow rates are normalized with respect to the value that gives a peak of 2 MPa. Here, the tensile strength does not add to the confining pressure and the air entry value. The irreversible opening of the discontinuity takes place above 2.5 MPa, while the sum of confining stress plus air entry value plus tensile strength gives: 1 + 0.3 + 0.5 = 1.8 MPa.

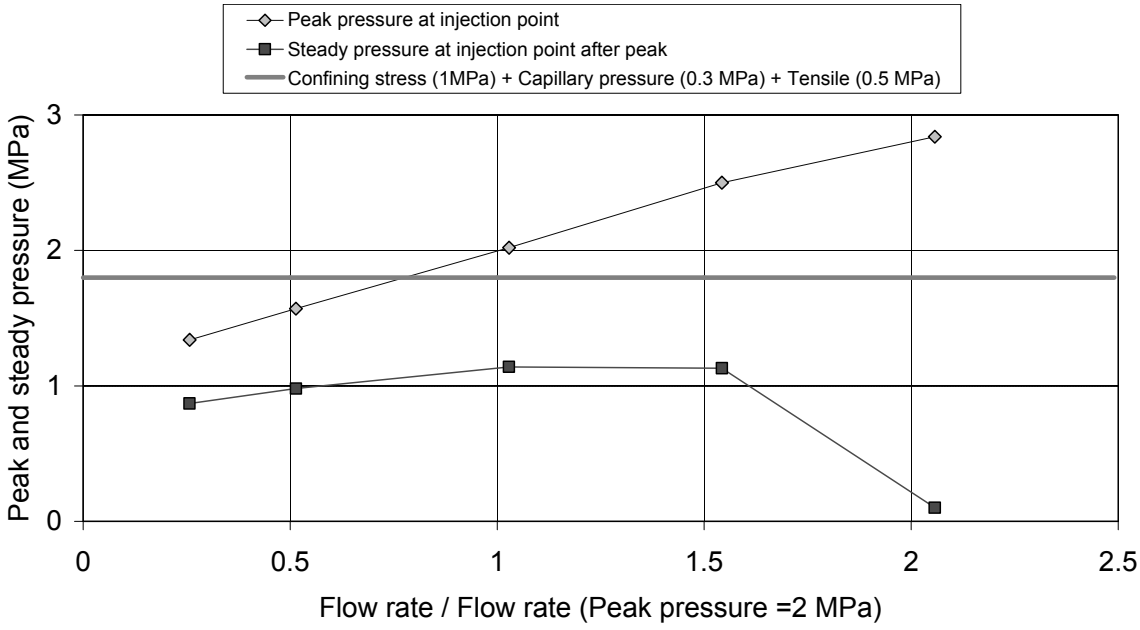

Fig. 10.- Peak and steady gas pressure at injection point for different tests at increasing injection gas flow rates.
Fig. 10.- Presión de gas pico y en condiciones estacionarias en el punto de inyección para diferentes ensayos a caudales de inyección de gas crecientes.

3.3. Concluding remarks

Using a few simple concepts of fracture development and the associated two phase flow phenomena along discontinuities, a continuum model capable of simulating flow in a fractured porous media has been developed. The calculation procedure is developed within the framework of a more comprehensive hydro-mechanical model for geological media. A realistic representation of irreversible fracture opening requires an elastoplastic constitutive model for the soil or rock skeleton. Fracture opening is characterized by two strain parameters: the threshold strain which marks the opening of the fracture and the tensile strain which marks the fracture in tension of the rock. Both can be equal in a simplified situation.

A few computer simulations, inspired in tests conducted to study gas flow through compacted clays and rocks have been presented. The analyses show the sensitivity of results to a number of factors controlling the tests usually performed. It is shown that the model reproduces in a natural way the peak discharge phenomena and peak gas pressure often reported in experiments. The model includes in a natural way two mechanisms which are generally present in a given experiment: two phase flow and concentrated flow through fractures. It is believed that the model developed offers good capabilities to solve in a realistic and relatively simple manner the complex phenomena of gas flow through fractured or potentially fractured media such as compacted clay buffers and host rock

4. Spatial heterogeneity of hydraulic and mechanical properties

4.1. Background

Delahaye and Alonso (2002) explored the effects of soil variability on gas migration. They presented results of numerical simulations of gas migration tests on saturated Boom clay, showing that the development of preferential paths may be a consequence of soil heterogeneity. These preferential pathways can be explained, in a deformable soil skeleton, by de action of a pressurized gas along a natural path defined in a spatially heterogeneous material by a set of connected spots of higher permeability. Soil undergoes marked desaturation along these paths and gas permeability increases fast.

In Delahaye and Alonso (2002) a procedure to simulate the material heterogeneity effects on gas migration process is described. Soil heterogeneity is defined by means of random fields of the key soil properties for gas migration. They generated two-dimensional stationary random permeability fields, described by a constant mean and a covariance function that depended only on the relative distance vector between two arbitrary points.

They studied several cases in order to perform a sensitivity analysis due to the lack of reliable data on soil heterogeneity. In the cases in which preferential paths were simulated satisfactorily, once the random permeability field was generated, the intrinsic permeability value was

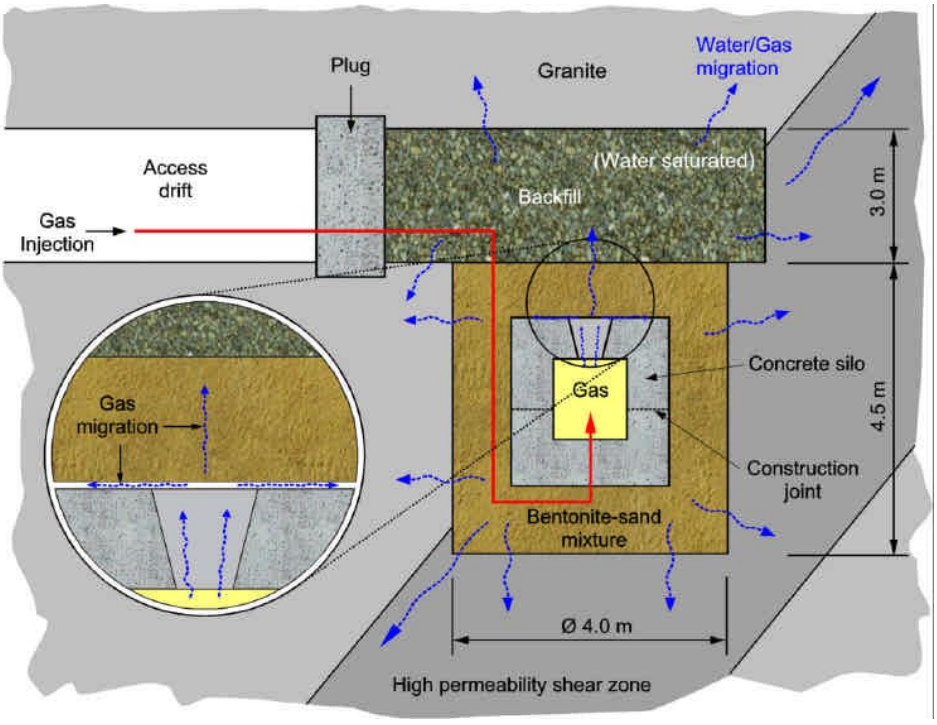

Fig. 11- GMT experiment concept (dimensions in meters).
Fig. 11- Concepto del ensayo GMT (dimensiones in metros).

linked to the element porosity through Kozeny's law. In addition, they related the air entry value from the retention curve, P_0, to soil porosity. Small porosity zones need higher suctions to start desaturation while higher porosity zones desaturate faster. The mechanical model played a key role in this work. The elastoplastic model considered to describe the mechanical behaviour of the soil (BBM, Alonso *et al*., 1990) permits the increase of porosity due to increasing gas pressure (decreasing net stresses).

This work is a proper background for the analysis reported in the subsequent sections of this paper. However, the model described for fracture opening, embedded in continuous finite elements will be used now to investigate gas path developments and changes in gas permeability. In addition, a computational case which mimics the conditions prevailing in the gas transmission zone of the large scale experiment GMT will be used to illustrate the mechanisms of gas flow through highly impervious barriers, initially saturated.

4.2. The large scale gas migration test GMT

4.2.1. Description

A large scale gas migration test was conducted by NAGRA (the Swiss radioactive waste management agency) at the Grimsel Test Site (Switzerland) from year 1998 to year 2003. Figure 11 shows a 2D scheme of the GMT test. An access drift and a vertical deposition hole were excavated in the granite rock. The engineered barrier (the cylindrical concrete silo and the compacted sand-bentonite mixture barrier) were built in place. Then the access drift was backfilled with sand. In order to saturate the compacted sand-bentonite barrier the system was pressurized at 0.55MPa with water coming from a pervious ring located at the backfill-barrier contact. This pressure was maintained constant throughout the test. Gas was injected inside the silo during several stages and it was allowed to escape through a mortar vent at the top of the silo, which also included a construction joint. The barrier was highly instrumented to detect stress and fluid pressure variations.

Figure 12 shows a detail of the engineered barrier. In a effort to detect the gas migration paths, layers 8 to 10 were traced with lead nitrate, $Pb(NO_3)_2$ and the injected gas was labelled with hydrogen sulphur, H_2S. The reaction between lead nitrate and hydrogen sulphur produces a dark mineral, galena (lead sulphide, PbS). Unfortunately, the addition of lead nitrate in the compaction water inhibited some of the swelling capacity of the bentonite, which resulted in higher permeability and higher stiffness of the sand-bentonite in layers 8 to 10.

A main zone for gas migration through the sand-bentonite barrier (layers 9 and 10, see Fig. 11) was identified during the experiment. Further data and interpretation of

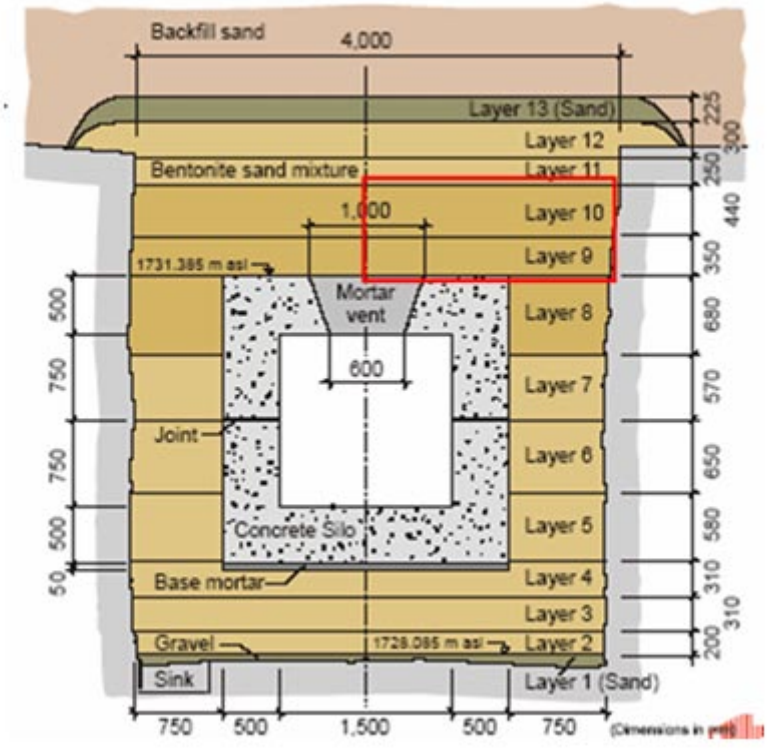

Fig. 12.- Detail of the GMT engineered barrier. Red rectangle indicates the domain selected for numerical simulations (dimensions in millimetres)
Fig. 12.- Detalle de la barrera de ingeniería del ensayo GMT. El rectángulo rojo indica el sector elegido para realizar las simulaciones numéricas (dimensiones in milímetros)

results is reported in the modelling analysis of GMT (Olivella and Alonso, 2005).

4.2.2. Modelling of the transmission zone

It was decided to focus the modelling simulations into the transmission zone incorporating the effects of the heterogeneity of hydraulic and mechanical properties of the sand-bentonite mixture. The discretized domain corresponds to the red rectangle area shown in figure 12. The simulations were conducted using CODE_BRIGHT (Olivella *et al.*, 1996) under plain strain conditions.

4.2.3. Boundary Conditions

Figure 13 shows the finite element mesh including a scheme of the boundary conditions considered in the analysis. A water pressure of 0.55 MPa was applied at the boundary (1) in order to simulate the pressurization and saturation stage of GMT. A prescribed mass flow of gas ($5.2 \cdot 10^{-6}$ kg/s, corresponding to the RGI-3b gas injection phase of GMT) was injected at the mortar vent boundary (2). Gas was allowed to escape through the boundary (1) when the gas pressure exceeded the prescribed water pressure of 0.55 MPa. The rest of the boundary was considered impervious.

Table 4 shows the steps considered in the analysis. The first phase lasted from day 1 to day 315. During this stage the barrier is progressively saturated. At day 315 gas injection begins.

The parameters of the constitutive model are shown in Tables 5 and 6. The mechanical model is an elasto-viscoplastic hardening model based on BBM (Alonso *et al.*, 1990) in which the behaviour of the soil depends on net stresses and suction. The embedded fracture model for permeability has been described in the previous section.

Time (days)	Step	BC
0-1	initial stress equilibrium	-
1-4	pressurization ramp (0-0.55MPa)	(1)
5-315(-4500)	constant water pressure (0.55MPa)	(1)
315-318	gas flux ramp (0-$6.2 \cdot 10^{-5}$ kg/s)	(2)
318-4500	constant gas flux ($6.2 \cdot 10^{-5}$ kg/s)	(2)

Table 4.- Analysis steps for GMT heterogeneous analysis.
Tabla 4.- Pasos para el análisis GMT heterogéneo.

Parameter	Value
E (MPa)	50
ν	0.35
κ	0.0001
κ_s	0.001
λ *(0)*	0.049
r	7.0
β (MPa-1)	70
k	0.03
p_0* (MPa)	0.26*
M	1.07

*mean value

Table 5.- Parameters of the mechanical constitutive model for GMT heterogeneous analysis.
Tabla 5.- Parámetros del modelo mecánico constitutivo para el análisis GMT heterogéneo.

Parameter	Value
Matrix intrinsic permeability, k (m^2)	$3.0 \cdot 10^{-16}$
Reference porosity	0.3
Initial fracture aperture, b_0 (m)	10^{-7}
Threshold strain, ε_0	10^{-3}

Table 6.- Parameters for the element permeability model. GMT heterogeneous analysis.
Tabla 6.- Parámetros para el modelo de permeabilidad. Análisis GMT heterogéneo.

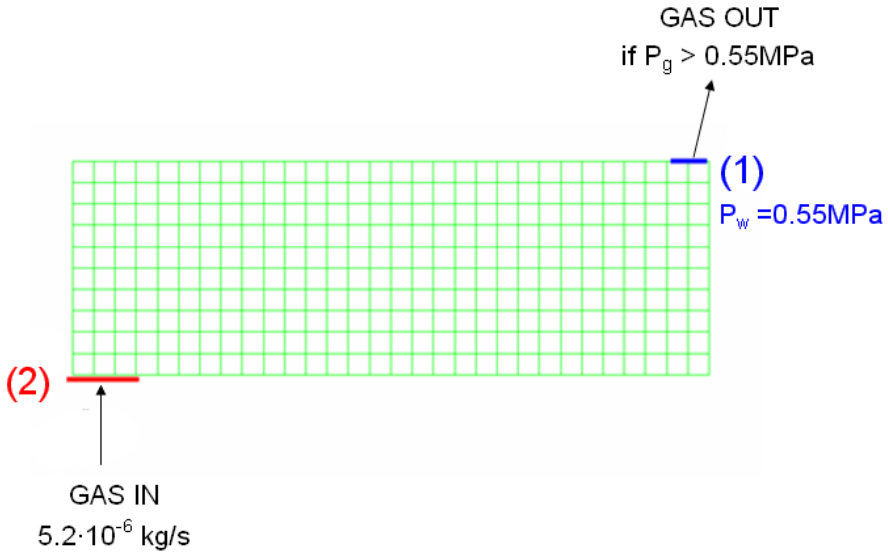

Fig. 13.- Scheme of the boundary conditions and finite element mesh.
Fig. 13.- Esquema de condiciones de contorno y malla de elementos finitos.

4.2.4. Simulation of soil heterogeneity

In order to simulate the sand-bentonite heterogeneity the following procedure was used. First a random porosity field is generated, having the same mean porosity as the barrier material (n = 0.3). Then, for each element, a volumetric deformation is computed from the mean void ratio, e_{mean} .

$$e = \frac{n}{1-n} \tag{7}$$

$$\varepsilon_v = -\frac{e - e_{mean}}{1 + e_{mean}} \tag{8}$$

The hardening parameter of the mechanical constitutive model, p_0*, is obtained as follows for each element:

$$p_0^* = p_{0mean}^* \exp\left(\frac{1 + e_{mean}}{\lambda - \kappa}\varepsilon_v\right) \tag{9}$$

Where λ and κ are the virgin and elastic compressibility parameters of the soil. It is important to note that porosity variations should be moderate in order to obtain realistic values of the hardening parameter following this procedure.

4.2.5. Results

Case 1

Figure 14 shows the initial porosity field considered in the first case presented. The mean value is 0.3 and the variance is in the order of 10^{-5}. This random field has a uniform distribution and it has no spatial correlation. Figure 15 shows the initial permeability field (log k) obtained from the porosity field by means of Kozeny's law (as initial fracture apertures are small). Note that, due to the small variations in porosity considered, initial permeability of all elements is in the same order of magnitude, so initially there is no marked heterogeneity in the hydraulic properties. This situation will change as the elements deform in response to changes in net stresses (ef-

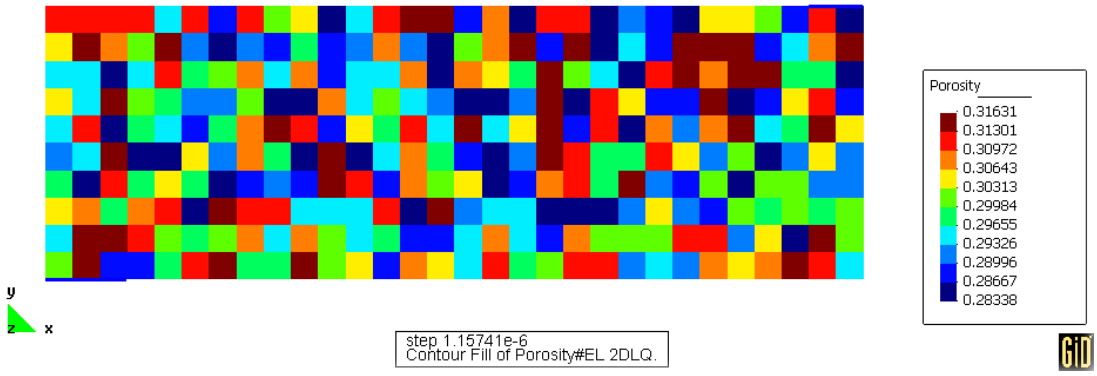

Fig. 14.- Initial porosity field. Case 1.
Fig. 14.- Campo inicial de porosidad. Caso 1.

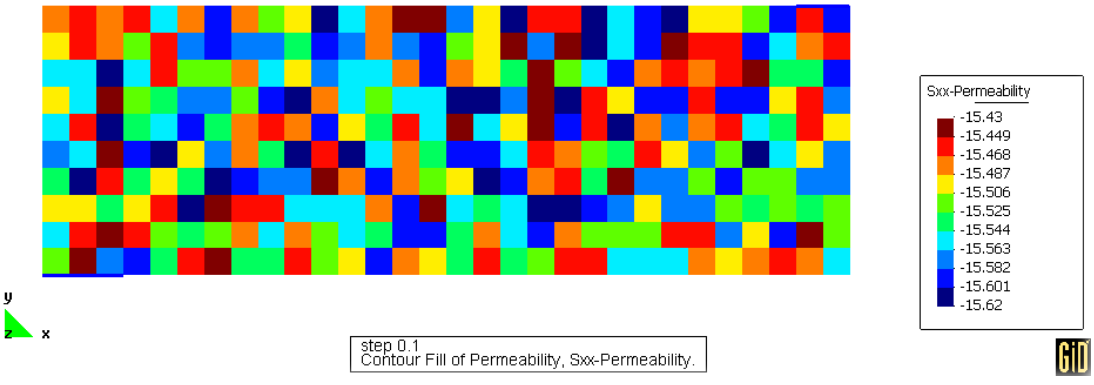

Fig. 15.- Initial permeability field (log *k*). Case 1.
Fig. 15.- Campo inicial de permeabilidad (log *k*). Caso 1.

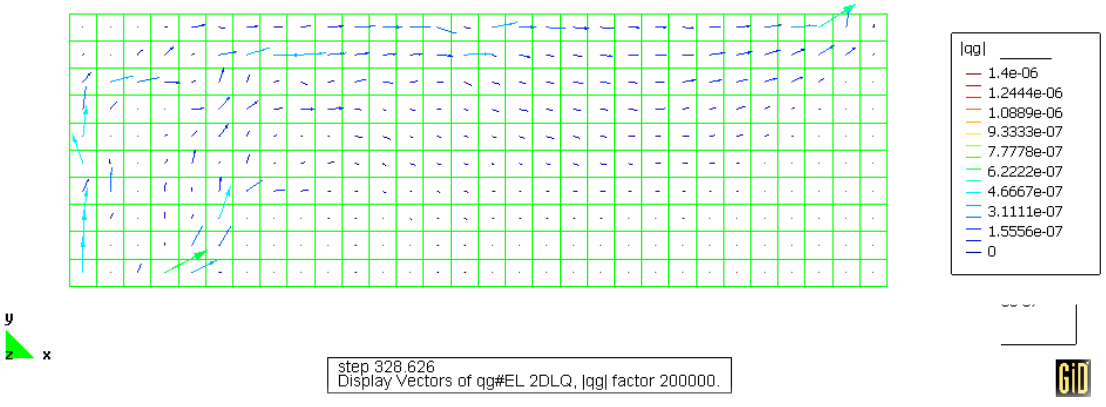

Fig. 16.- Advective gas fluxes (m/s). Case 1. Day 328.
Fig. 16.- Flujos advectivos de gas (m/s). Caso 1. Día 328.

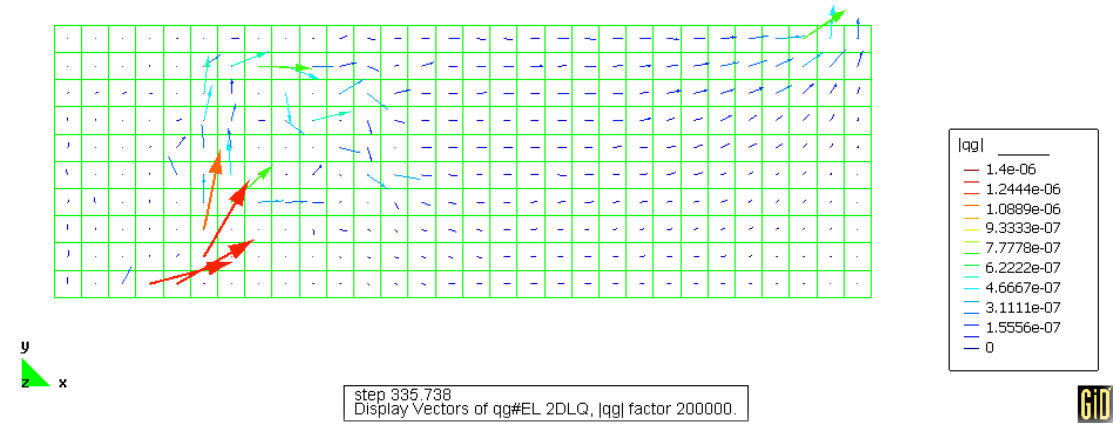

Fig. 17.- Advective gas fluxes (m/s). Case 1. Day 335.
Fig. 17.- Flujos advectivos de gas (m/s). Caso 1. Día 335.

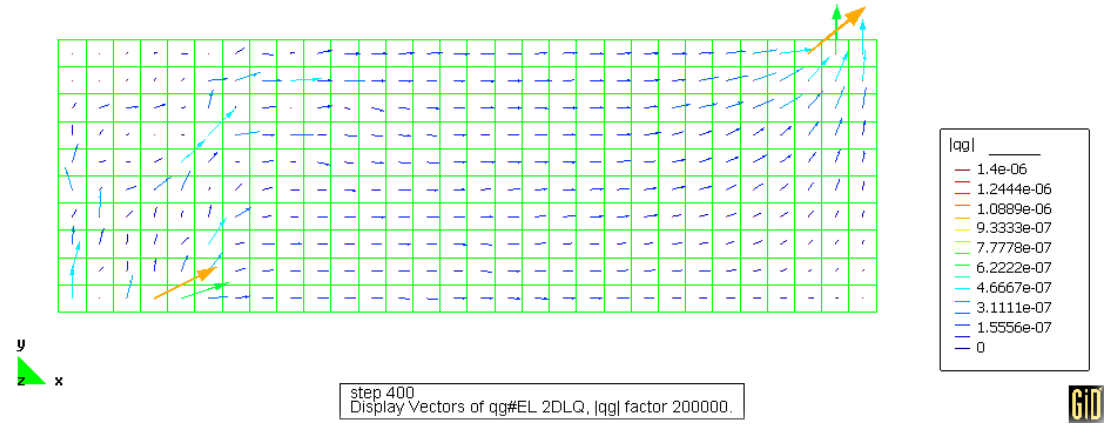

Fig. 18.- Advective gas fluxes (m/s). Case 1. Day 400.
Fig. 18.- Flujos advectivos de gas (m/s). Caso 1. Día 400.

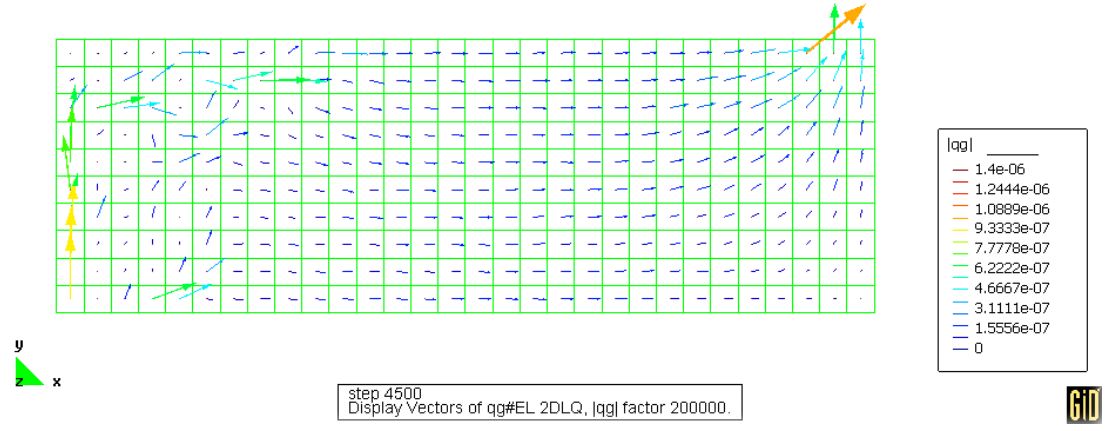

Fig. 19.- Advective gas fluxes (m/s). Case 1. Day 4500. End of the analysis.
Fig. 19.- Flujos advectivos de gas (m/s). Caso 1. Día 4500. Fin del análisis.

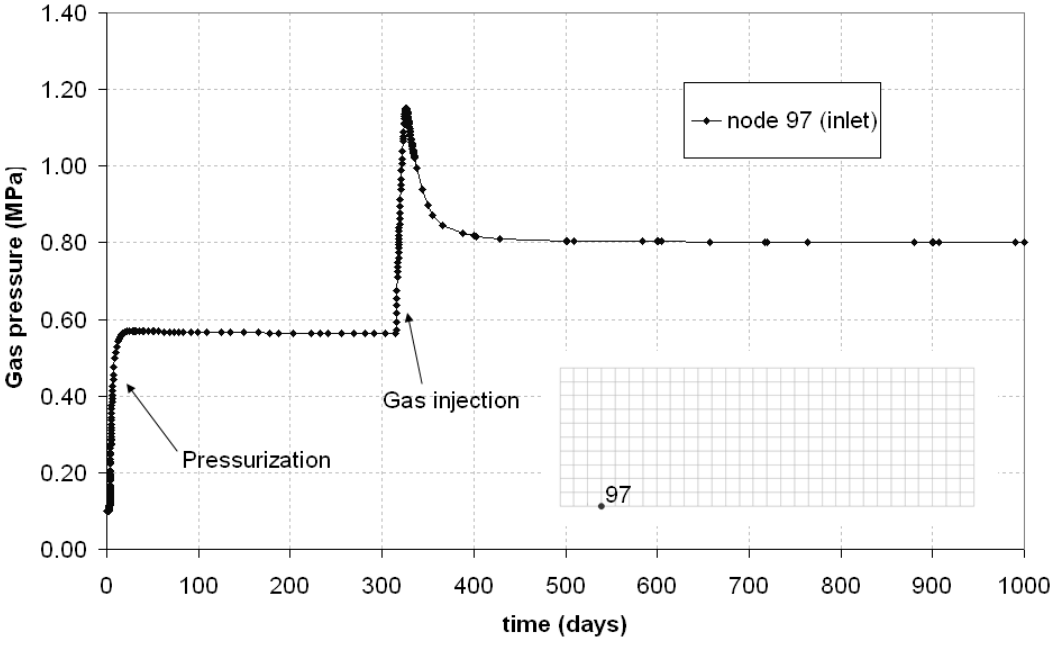

Fig. 20.- Evolution of gas pressure at node 97 (gas injection inlet). Case 1.
Fig. 20.- Evolución de la presión de gas en el nodo 97 (entrada del gas). Caso 1.

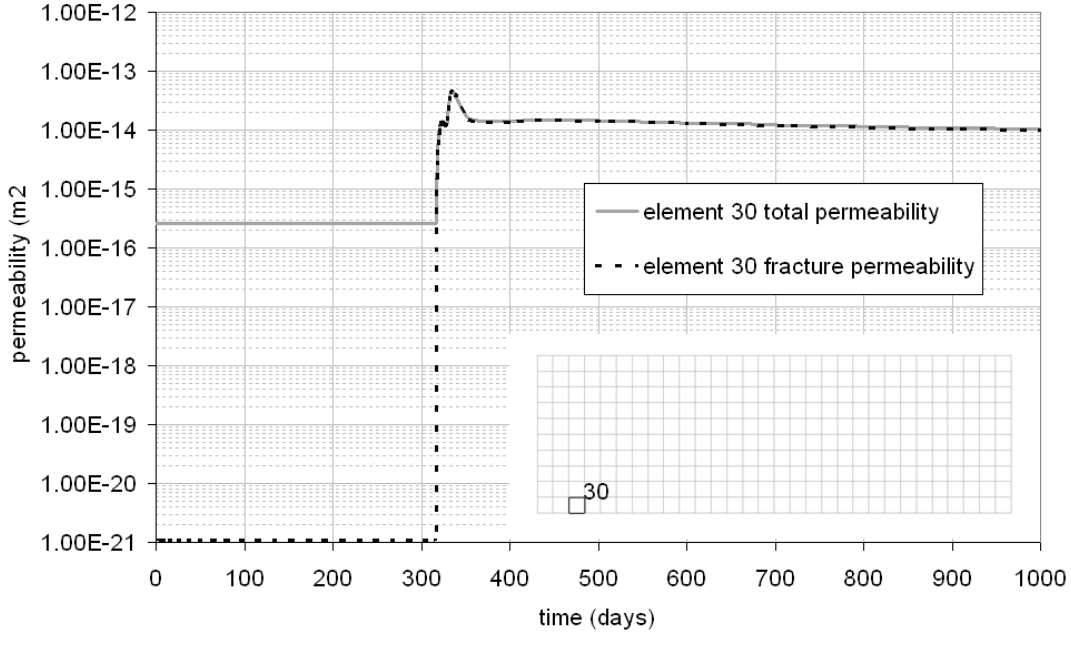

Fig. 21.- Evolution of permeability at element 30 (near gas injection boundary). Case 1.
Fig. 21.- Evolución de la permeabilidad en el elemento 30 (cerca del contorno). Caso 1.

fect of pressurization, saturation and gas injection).

Figure 16 shows the advective fluxes of gas (m/s) at day 328, showing the development of several gas paths. At day 335, after 20 days of gas injection, a marked preferential path has developed near the injection boundary (Fig. 17). This path becomes progressively closed (Fig. 18) and a new main path is developed from day 400 to the end of the analysis. Figure 19 shows gas fluxes at day 4500, once steady state has been reached.

The preferential paths developed do not progress through the soil to reach the outlet boundary. Compressive net stresses acting at the middle-right zone affect element

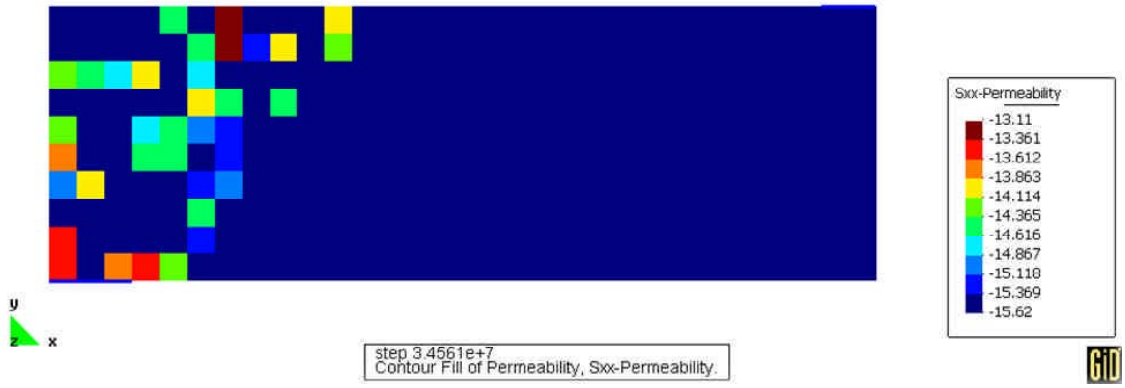

Fig. 22.- Permeablity field (log *k*) at day 400. Case 1.
Fig. 22.- Campo de permeabilidad (log *k*) en el día 400. Caso 1.

permeability as compression strains do not permit fracture opening. Gas transport in this zone becomes more homogeneous and this is clear in Figures 16 to 19.

The evolution of the gas pressure at node 97 (gas injection inlet) is shown in figure 20. Gas pressure shows a maximum during the gas injection stage, just as the threshold strain of some neighbouring elements is reached and the fracture aperture increases. Since permeability has substantially increased gas fluxes increase and therefore accumulated gas pressure is released, decreasing to a steady state value of 0.8MPa. Figure 21 shows the evolution of the permeability for element 30. Permeability increases more than 2 orders of magnitude due to the deformation undergone by the element (extension implies opening of the fracture in the permeability model once the threshold strain is exceeded). Figure 22 shows the permeability field at day 400.

Case 2

Figures 23 to 26 show the development of a preferential path obtained in a different simulation (flux vectors). The initial porosity field is a different realization of the same random field of the case presented above (uniform distribution, no spatial correlation). In this second case the main path formed did not close, and it progressed further than in the first case, reaching the top of the domain. In contrast, secondary paths change, as can bee seen in the sequence of figures.

Permeability field at day 4000 is shown in figure 27. Permeability along the preferential path has again increased 2 orders of magnitude. Note that permeability has raised 3 orders in some elements, although most of these elements have not been intersected by the main path.

The results presented in this section show that:

• It is necessary to introduce heterogeneity in order to obtain preferential paths for gas migration

• Main paths can close and other paths may develop

• Gas flows are 2-3 orders of magnitude higher in preferential paths

• Discharge peaks are a natural consequence of the model (rapid increase of fracture permeability imply a reduction of accumulated pressure)

Further modelling work may include the effect of soil anisotropy due to compaction procedures (i.e. higher correlation distance in horizontal direction), as well as actual soil heterogeneity data from laboratory (density values at some points, density variations) or from field measurements that could be related to porosity and permeability.

5. Summary

In the long term, once the compacted bentonitic barrier becomes saturated, the generation of gases in the canister may induce the development of preferential gas paths through the clay buffer. Experiments designed to reproduce the expected condition at laboratory scale have shown some characteristic features of this migration: a singular path opens when the gas pressure reaches the minimum principal total stress, the path opening coincides with a maximum applied gas pressure and a maximum discharge flow rate, which spontaneously decrease afterwards.

The paper describes a formulation for the simulation of preferential gas paths in a continuous medium. The approach may be implemented in existing THM codes, such as CODE_BRIGHT. The main idea is to embed a joint-like behaviour into a regular finite element. The flow and retention properties of the discontinuity are established by simple rules once the tensile strain normal to the discontinuity is known. This strain, in turn, depends on the constitutive law adopted for the continuum matrix.

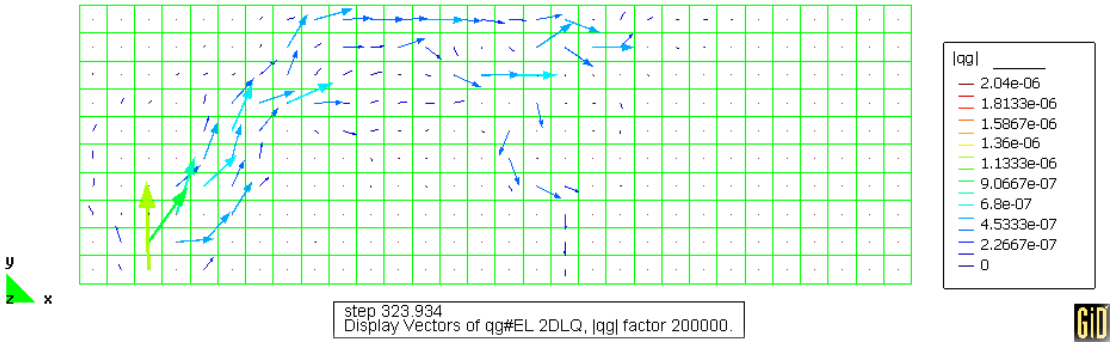

Fig. 23.- Advective gas fluxes (m/s). Case 2. Day 324.
Fig. 23.- Flujos advectivos de gas (m/s). Caso 2. Día 324.

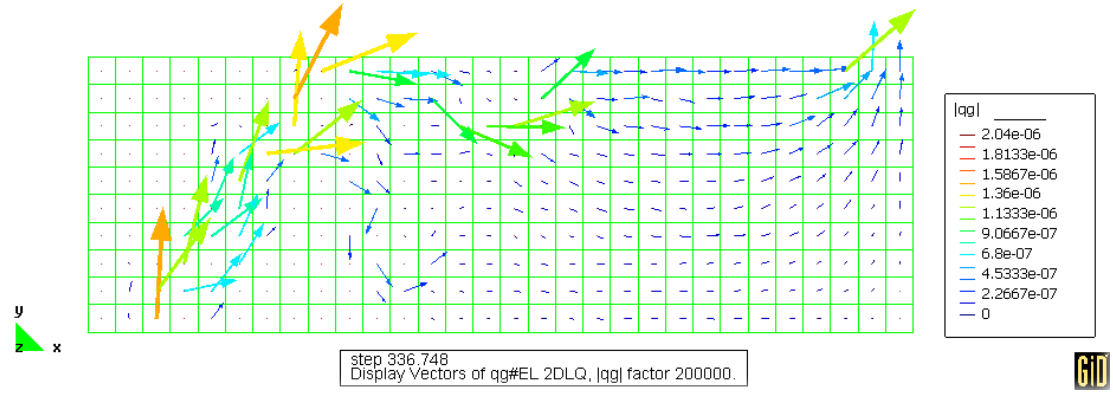

Fig. 24.- Advective gas fluxes (m/s). Case 2. Day 336.
Fig. 24.- Flujos advectivos de gas (m/s). Caso 2. Día 336.

Some examples presented show the capabilities of the formulation. The singular features of the tests mentioned may be appropriately simulated with the developed approach.

In a final part of the paper the effect of local heterogeneities in gas flow is examined. The approach was to simulate the behaviour of a randomly heterogeneous transmission zone. The geometry, material properties and boundary conditions are inspired in a recent large scale experiment (GMT) conducted in the Grimsel Rock Mechanics Laboratory. The variability of soil properties introduced in the simulation performed is rather weak. Nevertheless, their effect on gas migration is very relevant. All the soil elements were characterized by an embedded discontinuity in the sense described in the paper. The analysis has provided an additional insight on the mechanisms of gas transport in clay barriers. It was concluded that the formation of preferential paths requires some initial heterogeneity. It was also shown that paths may develop and close as a response to the changing stress state in the transmission zone. The existence of discharge peaks is a natural consequence of the formulation. The results are encouraging and may lead to more realistic computational procedures for the complex problem of gas migration through buffers.

References

Alonso, E.E., Gens, A., Josa, A. (1990): A constitutive model for partially saturated soils. *Géotechnique*, 40(3): 405-430.

Alonso, E.E. (1997): Flow and hydraulic fracture in earthfill dams. *Commission Internationale des Grands Barrages. 19th Congress*. Florence. Q73 R34, 521-549.

Alonso, E.E., Olivella, S., Delahaye, C. (2002): Gas Migration in Clays. *Environmental Geomechanics,* Lausanne: 83-94.

Alonso, E.E., Ledesma, A. (2004): *Advances in understanding engineered clay barriers*. Balkema. 583 pp.

Börgesson, L., Karnland, O., Johannesson, L.-E. (1996): Modelling of the physical behaviour of clay barriers close to water saturation. *Engineering Geology*, 41: 127–144.

Delahaye, C., Alonso, E.E. (2002): Soil heterogeneity and preferential paths for gas migration. *Engineering Geology*, 64: 251-271.

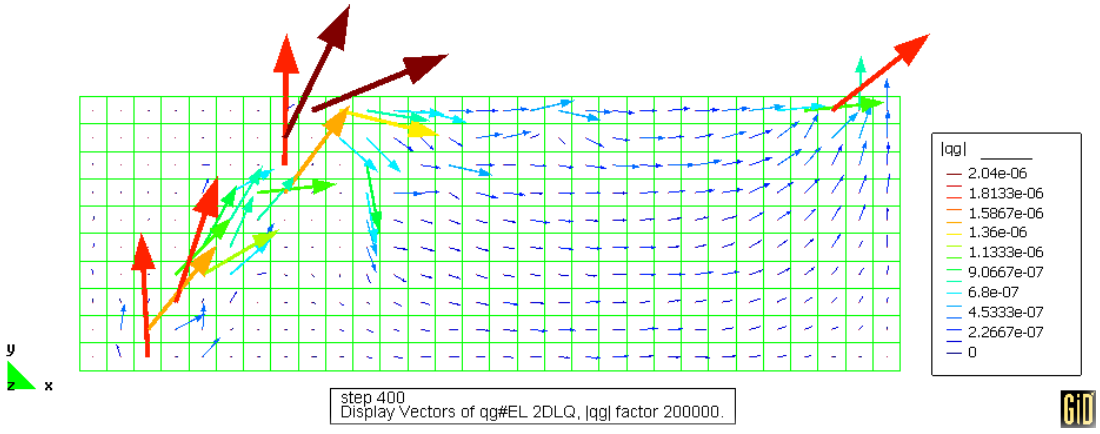

Fig. 25.- Advective gas fluxes (m/s). Case 2. Day 400.
Fig. 25.- Flujos advectivos de gas (m/s). Caso 2. Día 400.

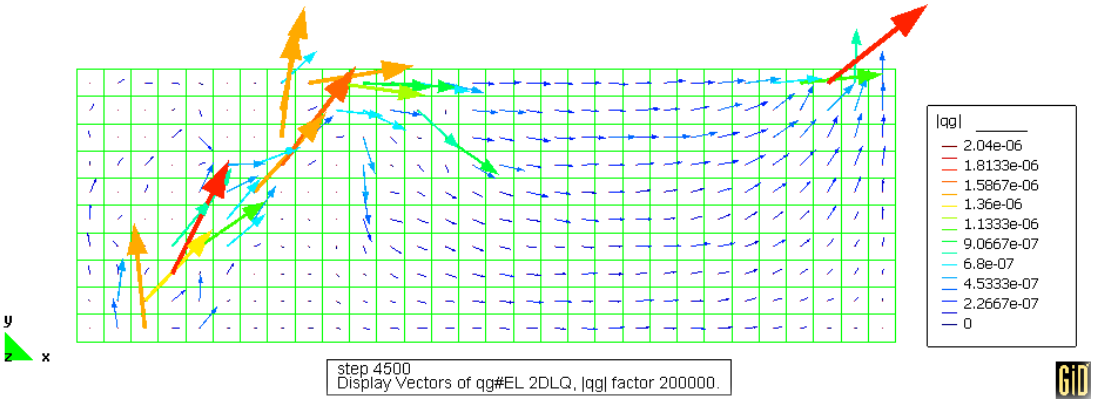

Fig. 26.- Advective gas fluxes (m/s). Case 2. Day 4500.
Fig. 26.- Flujos advectivos de gas (m/s). Caso 2. Día 4500.

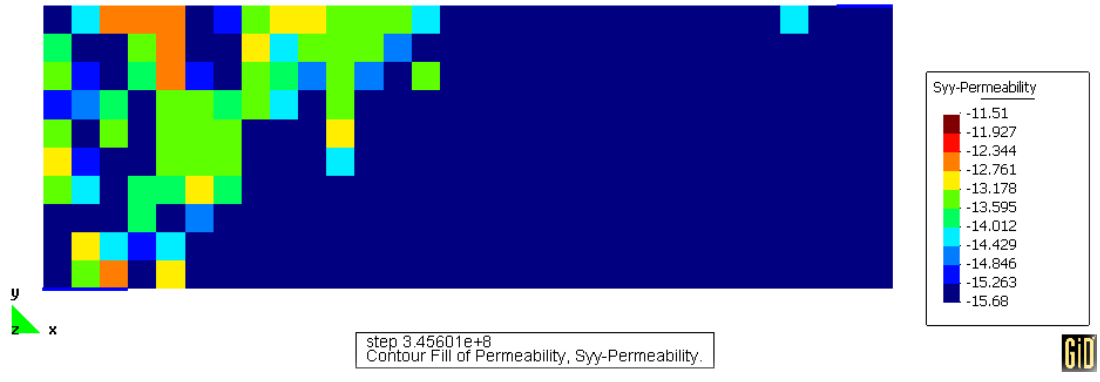

Fig. 27.- Permeablity field (log *k*) at day 4000. Case 2.
Fig. 27.- Campo de permeabilidades (log *k*) en el día 4000. Caso 2.

DIT-UPC (2000): CODE_BRIGHT. *A 3-D program for thermo-hydro-mechanical analysis in geological media. USER'S GUIDE*. Centro Internacional de Métodos Numéricos en Ingeniería (CIMNE), Barcelona.

Gens, A., Olivella, S., Valleján, B. (2001): Analysis of gas phase transport phenomena in compacted clay barriers. *Proceedings of the 10th International Conference on Computer Methods and Advances in Geomechanics*. Tucson, AZ, USA. 1: 735-742.

Graham, J., Gray, M., Halayko, K.G., Hume, H., Kirkham, T., Oscarson, D. (2002): Gas breakthrough pressures in compacted Illite and Bentonite. *Engineering Geology*, 64: 273-286

Horseman, S.T., Harrington, J.F. (1997): Study of gas migration in Mx80 buffer benonite. *BGS internal report WE/97/7 to SKB*.

Horseman, S.T., Harrington, J.F., Sellin, P. (1999): Gas migration in clay barriers. *Engineering Geology*, 54: 139-149.

Lee, H.S., Chou, T.F. (2002): Hydraulic Characteristics of Rough Fractures in Linear Flow under Normal and Shear Load. *Rock Mechanics and Rock Engineering,* 35(4): 299-318.

Olivella, S., Gens, A., Carrera, J., Alonso, E.E. (1995): Numerical formulation for a simulator (CODE_BRIGHT) for the coupled analysis of saline media. *Engineering Computations*, 13: 87-112.

Olivella, S., Alonso, E.E. (2005): Modelling the hydro-mechanical behaviour of GMT in situ test including interface elements. *Project Report 05-05*. Nagra.

Renner, J., Hettkaamp, T., Rummel, F. (2000): Rock mechanical characterization of an argillaceous host rock of a potential radioactive waste repository. *Rock Mech. Rock Engineering,* 33(3): 153-178.